

Global modeling of wall material migration following boronization in NSTX-U

J.H. Nichols¹, M.A. Jaworski², C.H. Skinner², F. Bedoya³, F. Scotti⁴, V.A. Soukhanovskii⁴, K. Schmid⁵

1 University of Tennessee – Knoxville, Knoxville, TN, USA

2 Princeton Plasma Physics Laboratory, Princeton, NJ, USA

3 Massachusetts Institute of Technology Plasma Science and Fusion Center, Cambridge, MA, USA

4 Lawrence Livermore National Laboratory, Livermore, CA, USA

5 Max-Planck-Institut für Plasmaphysik, Garching, Germany

Corresponding author:

Jacob H. Nichols (jnicho53@utk.edu)

108 Nuclear Engineering Building, 1412 Circle Drive, Knoxville, TN, 37996

Abstract

Boronization is commonly utilized in tokamaks to suppress intrinsic impurities, most notably oxygen from residual water vapor. However, this is a temporary solution, as oxygen levels typically return to pre-boronization levels following repeated plasma exposure. The global impurity migration model WalldYN has been applied to the post-boronization surface impurity evolution in NSTX-U. A “Thin Film Model” has been incorporated into WalldYN to handle spatially inhomogeneous conditioning films of varying thicknesses, together with an empirical boron conditioning model for the NSTX-U glow discharge boronization process. The model qualitatively reproduces the spatial distribution of boron in the NSTX-U vessel, the spatially-resolved divertor emission pattern, and the increase in oxygen levels following boronization. The simulations suggest that oxygen is primarily sourced from wall locations without heavy plasma flux or significant boron deposition, namely the lower and upper passive plates and the lower private flux zone.

1. Introduction

The control of impurities is a key factor in the performance of magnetic fusion devices, and the main source of impurities in a non-burning plasma is the tokamak vessel wall. Many tokamaks have reported improved plasma performance (see [1] and references within) following various wall conditioning techniques, primarily through lower radiated power and improved density control. One such conditioning technique is plasma-assisted chemical vapor deposition of boron, more commonly referred to as boronization. Conditioning with boron leads to the formation of a protective boron-containing layer on the plasma facing components (PFCs), which resists chemical erosion, getters oxygen from the plasma, and inhibits the release of gaseous impurities from the PFCs. In particular, NSTX [2] and NSTX-U [3] have boronized with deuterated trimethylboron (dTMB = $B(CD_3)_3$), which is less toxic and less explosive than other boron-containing gases. However, the positive effects of boronization are typically transient,

and it is unclear whether current conditioning techniques are compatible with long-pulse operation. This motivates the development of in situ conditioning techniques [4], as well as the development of models that can self-consistently predict the lifetimes of various conditioning techniques. This paper focuses on model development, applying the WalldYN mixed material migration code [5] to boronization in NSTX-U. WalldYN couples advanced models for surface processes (sputtering, reflection, deposition, and sublimation) and plasma impurity transport, and self-consistently calculates global migration due to multiple re-erosion and re-distribution steps while maintaining a global material balance. This makes it well-suited to inherently time-dependent and global-scale problems such as the surface evolution of PFCs during plasma exposure following wall conditioning.

2. The WalldYN model and recent improvements

The WalldYN model is described in detail in [5][6][7] so only the main concepts and new features of the model are presented here.

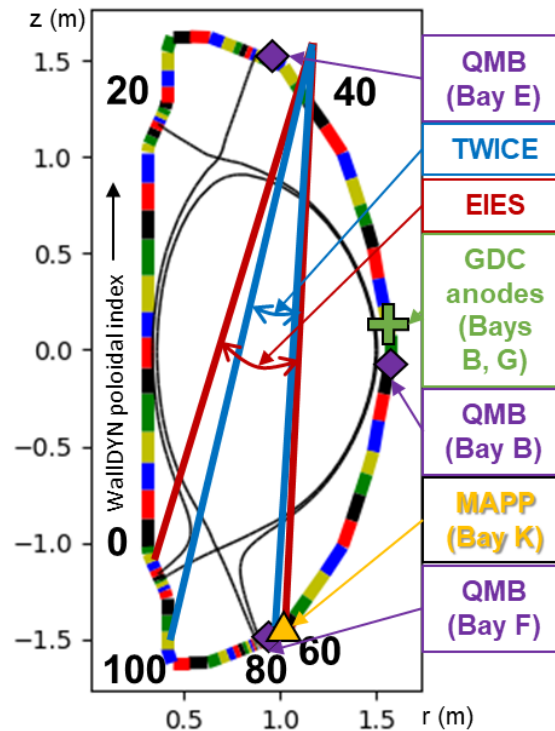


Figure 1: Wall discretization used for NSTX-U WalldYN simulations (alternating colors), with select bins labeled. Overlaid with magnetic configuration and important diagnostics: quartz crystal microbalances (QMBs), filtered fast camera view (TWICE), filterscope view (EIES), glow discharge anodes (GDCs), and Materials Analysis and Particle Probe (MAPP).

In a system with M elemental species, the tokamak wall is discretized into N components. The $N=115$ wall components used for the NSTX-U simulations of section 5 are shown as alternating colors in Figure 1. In previous WalldYN simulations, each wall component was modeled as a 2-layer system: a homogeneously mixed “reaction layer” of dynamic composition at the surface, in which all erosion/deposition processes occur, and a semi-infinite

“bulk layer” of fixed composition that interacts only with the reaction layer. The reaction layer represents the material that actually interacts with an incident particle, so the width is set to 1.5 times the average ion implantation depth for the system (approximately 40 Å for low Z materials). We assume that the average ion implantation depth is constant and independent of composition, which is a reasonable assumption for low-Z mixed materials, but may be inaccurate for high-Z material mixes. In the lab frame of reference, after net erosion occurs, an incident particle will interact with both the remnants of the reaction layer and the top portion of the bulk layer; similarly, net deposition leads to portions of the reaction layer becoming buried and unavailable for surface interactions. In the frame of reference of the fixed-width reaction layer itself, net erosion/deposition take the form of standard erosion/deposition fluxes at the surface, as well as apparent “exchange” fluxes to/from the bulk layer that serve to keep the total areal density of the reaction layer constant. The rate of change of areal density in the reaction layer for each element 1...M on each wall component 1...N is given by the balance of influxes to and effluxes from the wall, as well as the apparent exchange flux:

$$\frac{d\sigma_{wall,elem}^{REACTION}}{dt} = \sum_{charge} \Gamma_{wall,elem,charge}^{IN}(t) - \Gamma_{wall,elem}^{OUT}(t) \pm \Gamma_{wall,elem}^{EXCH}(t) \quad (1)$$

$$\Gamma_{wall,elem}^{EXCH}(t) = \begin{cases} -Conc_{elem,wall}^{REACTION} * |\Gamma_{wall}^{NET}(t)| & \text{Net deposition } (\Gamma_{wall}^{NET} > 0) \\ +Conc_{elem,wall}^{BULK} * |\Gamma_{wall}^{NET}(t)| & \text{Net erosion } (\Gamma_{wall}^{NET} < 0) \end{cases} \quad (2)$$

$$\Gamma_{wall}^{NET}(t) = \sum_{elem} \sum_{charge} \Gamma_{wall,elem,charge}^{IN}(t) - \Gamma_{wall,elem}^{OUT}(t) \quad (3)$$

One of the important improvements to the WalldYN model developed as part of this work, hereafter referred to as the “Thin Film Model” for reasons that will become apparent, is the introduction of a third “reservoir” layer in between the reaction layer and bulk for each wall segment. This reservoir layer has both a dynamic composition, and a finite dynamic width; in situations with strong erosion, it may even disappear. As before, all erosion/deposition processes occur homogeneously in a reaction layer of fixed width, so surface areal densities are still represented by Equation 1. However, the exchange flux now occurs between the reaction and reservoir layers, rather than the semi-infinite bulk:

$$\Gamma_{wall,elem}^{EXCH}(t) = \begin{cases} -Conc_{elem,wall}^{REACTION} * |\Gamma_{wall}^{NET}(t)| & \text{Net dep. } (\Gamma_{wall}^{NET} > 0) \\ \begin{cases} +Conc_{elem,wall}^{RESERVOIR} * |\Gamma_{wall}^{NET}(t)| & \sigma_{wall,tot}^{RESERVOIR} > \delta \\ +Conc_{elem,wall}^{BULK} * |\Gamma_{wall}^{NET}(t)| & \sigma_{wall,tot}^{RESERVOIR} < \delta \end{cases} & \text{Net ero. } (\Gamma_{wall}^{NET} < 0) \end{cases} \quad (4)$$

As a consequence of the finite extent of the reservoir layer, the layer may grow or shrink in time, and there are an additional M x N differential equations for areal densities in the layer:

$$\frac{d\sigma_{wall,elem}^{RESERVOIR}}{dt} = \begin{cases} +Conc_{elem,wall}^{REACTION} * |\Gamma_{wall}^{NET}(t)| & \text{Net dep. } (\Gamma_{wall}^{NET} > 0) \\ \begin{cases} -Conc_{elem,wall}^{RESERVOIR} * |\Gamma_{wall}^{NET}(t)| & \sigma_{wall,tot}^{RESERVOIR} > \delta \\ 0 & \sigma_{wall,tot}^{RESERVOIR} < \delta \end{cases} & \text{Net ero. } (\Gamma_{wall}^{NET} < 0) \end{cases} \quad (5)$$

In net erosion cases in which the total areal density of the reservoir has dropped below some threshold δ , the exchange flux occurs once again with the bulk (Equation 2). This model is discussed further in [8].

These additions enable the application of WalldYN to thin films. Films of arbitrary width, such as those generated during tokamak wall conditioning, can be modeled as the sum of the reaction and reservoir layers. Erosion of a wall coating is then represented by depletion of the

reservoir layer, eventually followed by the replacement of film atoms in the reaction layer with bulk atoms. Since the reservoir also keeps any codeposits buried during net deposition in the simulation, the Thin Film Model also allows WallDYN to model cases in which a single location transitions from net deposition to net erosion during the course of a simulation.

Rate parameters such as sputtering, reflection, and sublimation yields for mixed materials are obtained from scaling laws, which themselves are fit to experimental data (when available) or to the output of a large number of runs of SDTRIM.SP v. 5.07 [9], spanning all possible surface compositions. Chemical sputtering of carbon by deuterium is incorporated via the empirical formula of Roth [10]. Hydrogenic fluxes to the wall are obtained from EIRENE [11], and are assumed to be fixed in time. Impurity fluxes to each wall segment are treated as dynamic, and equal to the sum of fluxes eroded from other locations that end up transported to that wall segment:

$$\Gamma_{wall,elem,charge}^{IN}(t) = \sum_{source} R_{source,wall,elem,charge} * \Gamma_{source,elem}^{OUT}(t) \quad (6)$$

The redistribution matrix R , which represents impurity transport probabilities between all wall segments, is built up from the output of the 2D Monte Carlo impurity migration code DIVIMP [12]. Deposition probabilities are broken up by charge state, so that the incident particle spectrum is charge-resolved, and a realistic energy for ions (equal to $2kT_i + 3ZkT_e$) can be applied for sputtering/reflection. DIVIMP operates in the trace impurity approximation, so in WallDYN we assume that the hydrogenic plasma background remains fixed regardless of impurity content.

Equations of the form of Equations 1, 5, and 6 are written out for each wall segment, element, and charge state (where applicable), and are coupled into a differential-algebraic equation (DAE) system. The solution of this DAE system describes the dynamic evolution of surface areal densities and material fluxes to and from the plasma.

3. Boronization coverage model

Experimental characterization of boronization in NSTX-U has been reported in [3]. In this section, we present a brief summary, and describe an empirical boron deposition model.

NSTX-U is divided into 12 equal toroidal segments, labeled Bays A-L. Two glow discharge (GDC) electrodes are installed in the outer midplane sector of Bays B and G. Three quartz crystal microbalances (QMBs) [13] are installed for time-resolved deposition monitoring at Bays B mid, E top, and F bot (see Figure 1). During boronization, a helium GDC plasma is formed, with a gas mix of 95% He and 5% dTMB. ITER GDC modeling [14], as well as experimental results from JET and RFX [15], have shown that the ion current density is at least an order of magnitude higher near the anode compared to the rest of the vessel. This effect is clearly visible in NSTX-U as well, where an intense anode glow is observed near the electrodes on visible cameras during the GDC (see Figure 2a).

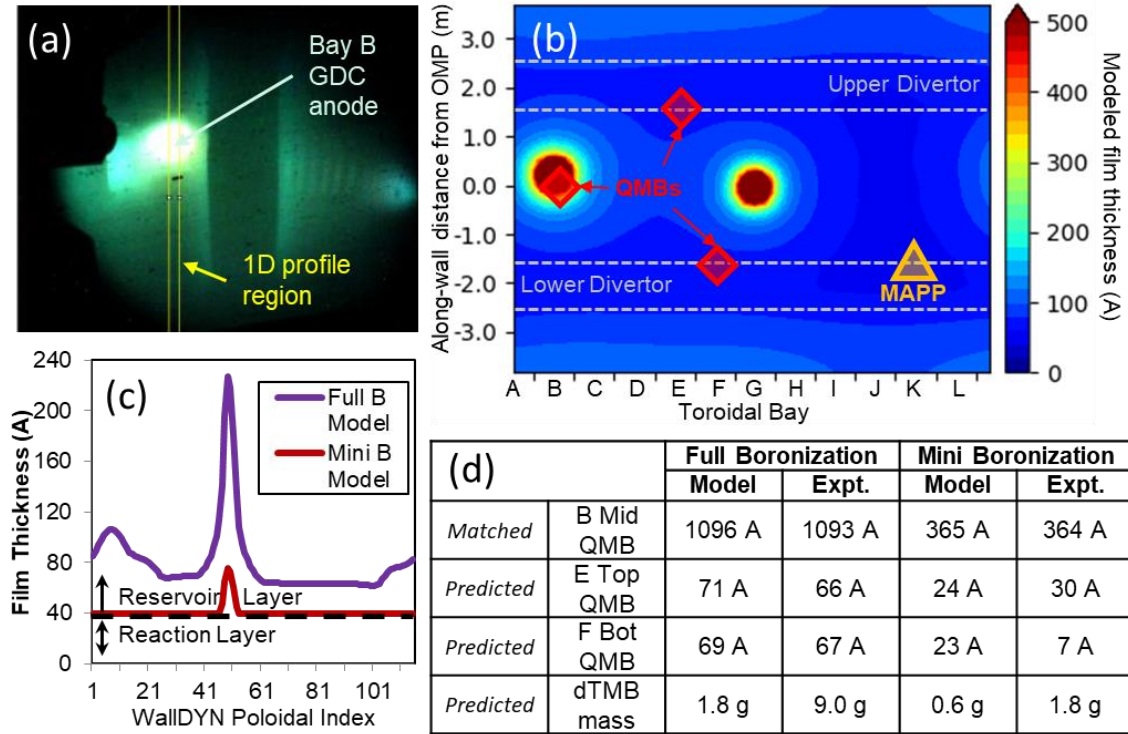


Figure 2: (a) Visible emission during NSTX-U boronization, with region used for 1D profile (yellow lines). (b) 3D map of modeled deposition during “full” boronization, with important locations labeled. (c) Film thicknesses, immediately after boronization, used as initial conditions in WalldYN simulations. (d) Comparison of boronization coverage model with experimental measurements.

Two different boronization regimes were used in the 2016 NSTX-U campaign [16]: “full” boronizations, which used a full bottle (9.0 g) of dTMB, and “mini” boronizations, which used 1/5 bottle (1.8 g) of dTMB. Typically, full boronizations were applied on a weekly basis, while mini boronizations were applied nightly later in the campaign.

Following each boronization, the lower divertor Materials Analysis and Particle Probe (MAPP) [17] consistently measured a surface composition of approximately 35% B, 60% C, and 5% O. We assume that this composition is representative of the boron-conditioned surface layer throughout the device, with only the thickness of the layer varying in space. The MAPP composition measurement represents an enrichment of boron compared to dTMB, which contains 3 C atoms per B atom; this is likely due to details of the dTMB breakup process, which is beyond the scope of this empirical model. Prior to boronization, MAPP measured a composition of 80% C and 20% O. This composition is used for the semi-infinite bulk layer in WalldYN.

To establish an empirical deposition thickness model during the GDC plasma, it is assumed that ion current density, and thus deposition thickness, is proportional to light emission intensity. In the absence of local measurements, a 1D profile of emission versus distance to electrode is extracted from the wide-angle camera image in Figure 1a. A 3D map of deposition probability is formed by summing the contributions from each GDC electrode, based on the distance to each wall segment. Assuming a boron concentration in the layer of 35%, the

total number of boron atoms is scaled such that the total film thickness at the Bay B mid QMB location matches the experimental measurement, creating a 3D map of film thickness (Figure 2b). The film thickness at the other QMB locations can then be used to evaluate the model. As seen in Figure 2d, agreement is quite good at the E top and F bot QMBs. However, the model only requires 20-35% of the total injected dTMB to reproduce the observed film thicknesses. This discrepancy is likely due to 2 effects: dTMB that doesn't deposit on the main wall, and instead is deposited in recessed areas; and potentially enhanced deposition in the immediate vicinity of the GDC electrode, which is not well resolved in this simple empirical model.

The resulting thickness of the boron-conditioned layer is highly localized within approximately 1 m diameter around the GDC electrodes, and is nearly constant throughout the rest of the device. This boronization coverage model is used as an initial condition for WalldYN, after toroidal averaging is applied. Figure 2c shows the thickness profiles for full and mini boronizations versus poloidal index, with the reaction and initial reservoir layers demarcated. It turns out that the results presented in section 5 are insensitive to toroidal variations in films thickness, since films outside the outer midplane sector are approximately toroidally symmetric.

4. NSTX-U plasma model

The scrape-off layer (SOL) background plasma solution is a key input to the WalldYN model, both directly through hydrogenic fluxes and energies, and indirectly through DIVIMP redistribution probabilities. Thus, one would ideally have a background plasma for each plasma state present during the times of interest. Unfortunately, the 2016 NSTX-U campaign was cancelled before many of the diagnostics that would be required for a direct reconstruction of NSTX-U plasmas were fully operational (most notably Langmuir probes). Thus, we make use of a proxy plasma solution that approximates plasma conditions and locations during the 2016 NSTX-U campaign.

The magnetic equilibrium for our proxy plasma is taken from NSTX-U discharge 204980, a moderately lower single null ($dR_{sep} = -8$ mm) shape with high X-point and low triangularity. This was the most common shape during the campaign, and the inner and outer strike points locations are representative of average locations over the campaign [8]. An extended computational grid, which fills gaps between the wall and primary SOL with field-aligned flux tubes, is generated for this equilibrium using GRID [18].

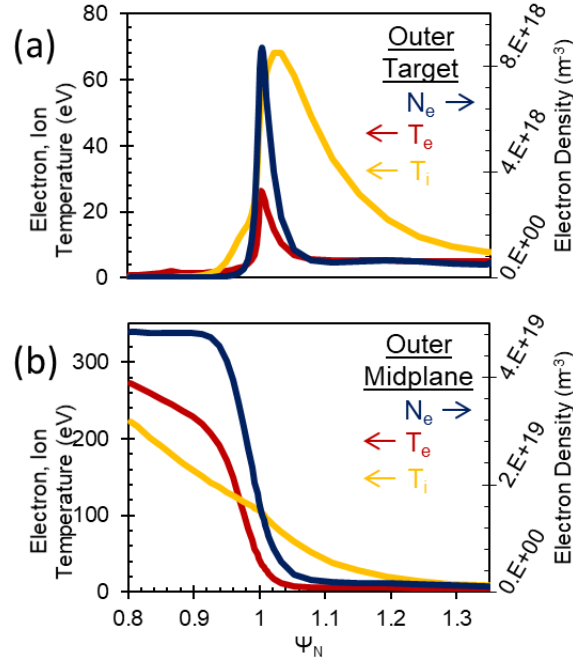


Figure 3: Outer target (a) and outer midplane (b) plasma parameters for NSTX-U H-mode proxy plasma background, versus normalized magnetic flux.

The plasma conditions for the NSTX-U proxy plasma are modeled after validated SOLPS simulations of NSTX boron conditioned discharges [19][20]. Target and midplane plasma parameters, Figure 3, are extracted from the NSTX SOLPS results (versus normalized magnetic flux), and used as boundary conditions for OSM-EIRENE [12] calculations in the NSTX-U geometry. OSM-EIRENE provides a good match to SOLPS along the outer leg of the SOL. Outer leg plasma profiles are mirrored to the inner leg in order to generate an attached solution; the influence of divertor detachment on material migration is an important question that needs to be addressed, but is beyond the scope of this paper. NSTX operated prior to 2011 with a similar geometry to NSTX-U, utilizing both lithium and boron wall conditioning; datasets from the boron phase of NSTX are chosen to eliminate the interference of pedestal modifications due to lithium conditioning [20], which may affect impurity transport. NSTX discharge 129015, a 4 MW NBI-heated H-mode, is generally representative of the line-averaged densities and plasma stored energies (W_{MHD}) of the highest-performing 10% of NSTX-U discharges; since the rate of plasma-material interactions are expected to roughly scale with W_{MHD} , this means that our simulations likely represent an upper bound for material evolution rates in the actual 2016 NSTX-U campaign.

5. Results

The aim of this work is to validate the WalldYN model through comparison to the evolution of post-boronization experimental observables. The clearest experimental trend is the immediate suppression of oxygen emission following boronization, followed by a gradual return to pre-boronization levels after plasma exposure. Figure 4 shows the lower divertor oxygen emission as a function of time after boronization, measured by the EIES filterscope

system [21]. The field of view of the filterscope can be seen in Figure 1. The OII emission (4419 Å) is normalized by the D-γ emission (4334 Å) in order to minimize variability due to different plasma configurations. The OII recovery rate is surprisingly consistent across different boronizations, with different plasma conditions. However, one key difference is full versus mini boronizations, described in section 3: OII recovers notably faster following mini boronizations.

Synthetic diagnostics have been incorporated in WalldYN for comparison to NSTX-U spectroscopic results. Plasma impurity densities are converted to photon emission via ADAS photon emission coefficients [22], and integrated along lines of sight and averaged across the view cone. Since the spectroscopic diagnostics could not be absolutely calibrated without Langmuir probes, a direct comparison with the model is not possible. Instead, the WalldYN OII/D-γ traces are multiplied by an arbitrary factor (2.5 in this case) to match the experimental signals at $t=0$. Figure 4 also shows the WalldYN Thin Film Model results, using both the mini and full boronization initial conditions. There is a clear bifurcation between the two cases, similar to what is observed experimentally, which is not produced in WalldYN without the Thin Film Model. Additionally, the full boronization simulation reproduces the slow change in OII emission during the first 5 seconds of plasma exposure after boronization, and the rollover in OII emission after long exposure times.

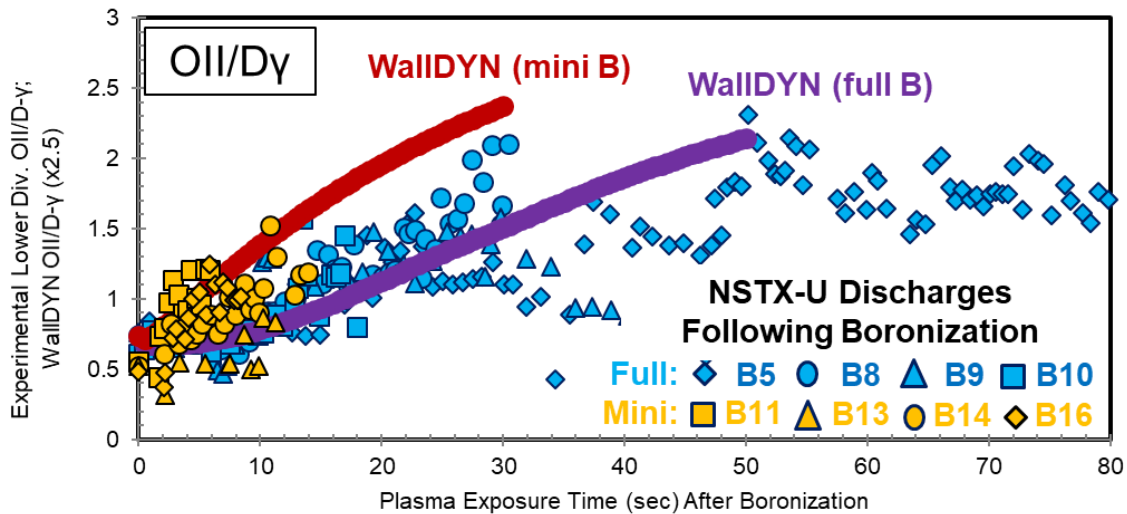


Figure 4: Measured lower divertor OII/Dγ emission following boronizations in NSTX-U. WalldYN Thin Film results using the full/mini boronization models (multiplied by 2.5) are overlaid.

Lower divertor CII emission (5143 Å) shows very little temporal evolution when normalized by D-γ. This lack of evolution is also observed in WalldYN Thin Film Model simulations, with both mini and full boronizations.

Filtered fast cameras, such as the TWICE system installed on NSTX-U [23], provide improved spatial resolution over filterscope arrays. However, since current NSTX-U WalldYN simulations are limited to proxy plasmas, a direct comparison with measured camera profiles is not meaningful. However, important information about the surface state can be extracted by measuring the change in emission observed when running the same plasma configuration at different times. Figure 5a shows TWICE emission profiles from an identical L-mode configuration, run at the beginning of the day (after an overnight mini-boronization), and at the

end of the day following 13 seconds of plasma exposure (20 discharges). The oxygen signal has increased considerably, consistent with the filterscope observation. The boron signal has also dropped, while the carbon signal remained effectively unchanged. Figure 5b shows WalldYN simulations at similar points in time, following a mini-boronization and using the H-mode proxy plasma. While the profile shapes show obvious differences (due to the difference in gradients between H-mode and L-mode), the relative changes in surface emission are in good agreement with those observed in experiment.

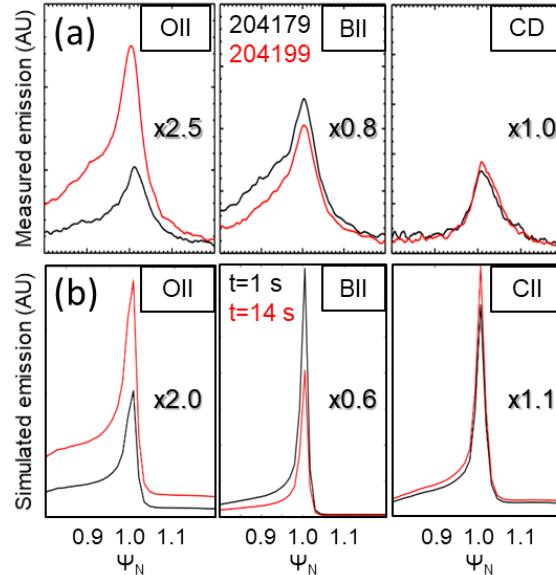


Figure 5: (a) Measured spatially-resolved divertor emission for identical discharges, immediately after mini boronization #14 and after 13 seconds plasma exposure. (b) Simulated divertor emission after an equivalent plasma exposure time. Relative changes in emission profiles are listed numerically.

The Material Analysis and Particle Probe (MAPP), installed in the lower outer divertor, also observed an increase in surface oxygen during post-boronization plasma exposure [3][17]. This trend is qualitatively reproduced with WalldYN, but the rate is underestimated by a factor of 2. It turns out that the oxygen impurity evolution rate calculated by WalldYN in the far SOL (where MAPP is located) is rather dependent on the distance to the strike point, with oxygen evolution rates in line with MAPP observations found closer to the separatrix. This finding suggests that a more careful consideration of strike point motion during a discharge may be necessary for future quantitative comparisons that include MAPP data.

6. Discussion

Given the apparent reasonable agreement between WalldYN modeling of wall oxygen evolution and NSTX-U experimental observables, it may be useful to delve deeper into the models for insights beyond experiments. In general, the rise in surface oxygen in WalldYN simulations is due to oxygen originating in the bulk layer, which is released when the thin film overlayer erodes away. However, this process is not spatially uniform, and some parts of the wall are regions of net oxygen deposition that sequester oxygen out of the plasma. As seen in Figure 6, when integrating over toroidal space and time, the primary sources of oxygen in the

WalldYN simulation are the lower passive plates, upper passive plates, and lower private flux zone. Meanwhile, low levels of oxygen are sequestered by codeposition in high flux regions, such as the strike points. In all, over 50 seconds of plasma exposure, the simulated plasma+surface system sees a net increase of 1.4×10^{21} O atoms, equivalent to 37 mg of O_2 gas.

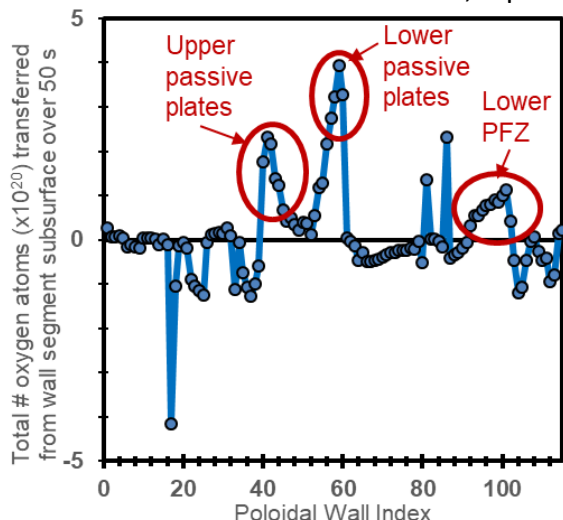


Figure 6: Toroidally-integrated oxygen atoms transferred from the bulk, over 50 seconds, in full boronization WalldYN simulations.

Since the rate of oxygen evolution appears to be relatively independent of plasma configuration, one might question whether the evolution is due to chemical oxidation due to ambient gases, rather than plasma-induced erosion. However, every discharge following mini-boronization #12 was the same configuration, a low-power L-mode used for error field testing, and no change in impurity signals (including oxygen) was observed throughout the day. If the oxygen evolution was truly plasma-independent, an increase in oxygen would have been observed even when running this low-performance scenario. All other operations days had a mix of high- and low-performance discharges, and did observe oxygen evolution. More work needs to be done to understand the apparent threshold effect, since pure-material sputtering data for deuterium on boron suggests that even this low-power plasma should result in some level of physical sputtering.

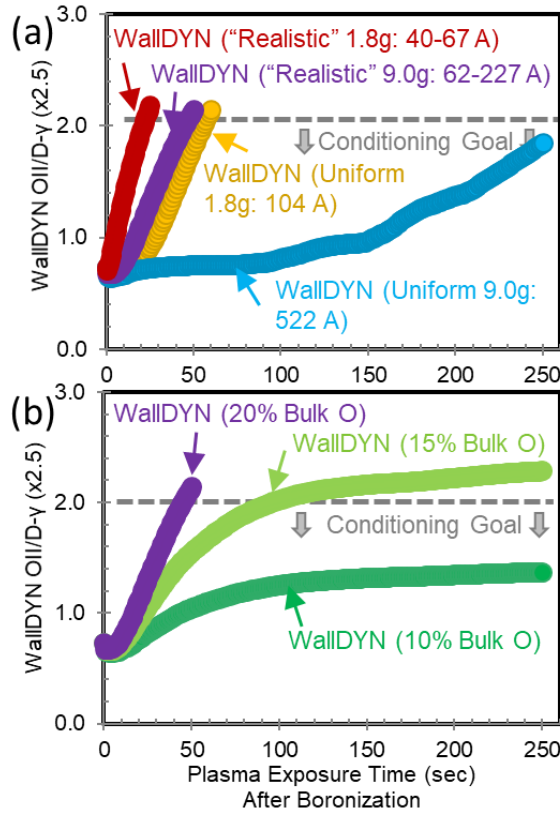


Figure 7: Simulated OII/Dy emission under different (a) coating uniformity conditions, and (b) bulk oxygen content conditions. Plasma performance typically drops when OII/Dy ≥ 2.0 .

Simulations such as those presented in section 5 can also be used to design operational improvements. For instance, what would be the result with a perfectly uniform film? Figure 7a shows the oxygen evolution from cases with identical plasma conditions, but different initial film uniformity. The “realistic” full and mini boronization cases are reproduced from Figure 4, and the oxygen level above which plasma performance is significantly degraded is shown as a horizontal line. When 1.8g dTMB is uniformly distributed as a 104 A film, the coating lasts 60 seconds – longer than the current 9.0g dTMB coating. When this 9.0g dTMB coating is uniformly distributed as a 522 A film, simulations suggest that the wall would stay well-conditioned for over 250 seconds of plasma exposure. With such a uniform coating, oxygen from sources such as the upper and lower passive plates (Figure 6) stays coated by the boron thin film for a much longer period of time. Similarly, tokamak operators strive to reduce oxygen inventory in the PFCs through techniques such as bakeouts and GDC cleaning. This can be modeled in WallDYN by changing the oxygen composition in the bulk layer. Figure 7b shows oxygen evolution for a current full boronization, but under 3 bulk oxygen regimes: 20% (same as Figure 4), 15%, and 10%. A lower bulk oxygen concentration leads to both slower oxygen uptake, and lower equilibrium surface oxygen content.

7. Conclusions

The global mixed material migration code WallDYN has been compared to post-boronization impurity evolution measurements in NSTX-U. Good qualitative agreement is

found, reproducing the different rates of wall de-conditioning observed during plasma operations following conditioning with different amounts of boron-containing gas. This agreement is only possible when using the new “Thin Film Model” for WalldYN, presented in this work, which adds a “reservoir” layer in between the surface reaction layer and the nonreactive bulk. With this capability, WalldYN can be applied to systems with mixed-material thin (4-1000 nm) films, such as those frequently encountered in wall conditioning scenarios. For impurity evolution in NSTX-U, future experiments are required to make quantitative comparisons with the WalldYN model, but preliminary conclusions can be drawn from the current work. For instance, simulations suggest that oxygen is primarily sourced from wall locations without heavy plasma flux or significant boron deposition, namely the lower and upper passive plates and the lower private flux zone. In future work, it will be important to evaluate how sensitive this analysis is to the specifics of the plasma configuration. Still, this motivates continued efforts to optimize the wall conditioning process through more uniform boron deposition, and more complete vessel bakeouts of residual water vapor.

Acknowledgements

This work was supported by US DOE contract DE-AC02-09CH11466, as well as EURATOM within the framework of the European Fusion Development Agreement.

References

- [1] J. Winter, Plasma Phys. Control. Fusion 38 (1996) 1503-1542
- [2] C.H. Skinner, et al., Nucl. Fusion 42 (2002) 329-332
- [3] C.H. Skinner, et al., Nucl. Mater. Energy 12 (2017) 744-748
- [4] A. Bortolon, these proceedings
- [5] K. Schmid, et al., J. Nucl. Mater. 415 (2011) S284-S288
- [6] K. Schmid, et al., Nucl. Fusion 55 (2015) 053015
- [7] K. Schmid, et al., J. Nucl. Mater. 463 (2015) 66-72
- [8] J.H. Nichols, “Integrated Modeling of Plasma-Induced Material Migration in NSTX-U”, PhD Thesis, Princeton University, 2018.
- [9] A. Mutzke, et al., “SDTrimSP Version 5.00”, IPP Report 12/8 (2011)
- [10] J. Roth, J. Nucl. Mater. 266-269 (1999) 51-57
- [11] D. Reiter, et al., Fusion Sci. Tech. 47 (2005) 172-186
- [12] P.C. Stangeby, et al., J. Nucl. Mater. 313-316 (2003) 883-887
- [13] C.H. Skinner, et al., J. Nucl. Mater. 363-365 (2007) 247-251
- [14] G.J.M. Hagelaar, et al., Plasma Phys. Control. Fusion 57 (2015) 025008
- [15] D. Kogut, et al., Plasma Phys. Control. Fusion 57 (2015) 025009
- [16] D.J. Battaglia, et al., Nucl. Fusion 58 (2018) 046010
- [17] F. Bedoya, et al., Nucl. Mater. Energy 12 (2017) 1248-1252
- [18] S.W. Lisgo, et al., J. Nucl. Mater. 438 (2013) S580-S584
- [19] J.M. Canik, et al., Phys. Plasmas 18 (2011) 056118
- [20] J.M. Canik, et al., J. Nucl. Mater. 415 (2011) S409-S412
- [21] V.A. Soukhanovskii, “National Spherical Torus Experiment Upgrade Edge Impurity Emission Spectroscopy (EIES) aka Filterscopes”, Accessed May 2017:
http://nstx.pppl.gov/DragNDrop/Operations/Diagnostics_&Support/Sys/EIES/

[22] H.P. Summers, et al., “ADAS manual 2.6”, Accessed Dec 2017:

<http://www.adas.ac.uk/manual.php>

[23] F. Scotti and V.A. Soukhanovskii, Rev. Sci. Instrum. 86 (2015) 123103